LETTER

doi:10.1038/nature16153

Thermal vesiculation during volcanic eruptions

Yan Lavallée[1], Donald B. Dingwell[2], Jeffrey B. Johnson[3], Corrado Cimarelli[2], Adrian J. Hornby[1], Jackie E. Kendrick[1], Felix W. von Aulock[1], Ben M. Kennedy[4], Benjamin J. Andrews[5], Fabian B. Wadsworth[1,2], Emma Rhodes[4] & Gustavo Chigna[6]

Terrestrial volcanic eruptions are the consequence of magmas ascending to the surface of the Earth. This ascent is driven by buoyancy forces, which are enhanced by bubble nucleation and growth (vesiculation) that reduce the density of magma[1]. The development of vesicularity also greatly reduces the 'strength' of magma[2], a material parameter controlling fragmentation and thus the explosive potential of the liquid rock[3]. The development of vesicularity in magmas has until now been viewed (both thermodynamically and kinetically) in terms of the pressure dependence of the solubility of water in the magma, and its role in driving gas saturation, exsolution and expansion during decompression. In contrast, the possible effects of the well documented negative temperature dependence of solubility of water in magma has largely been ignored. Recently, petrological constraints have demonstrated that considerable heating of magma may indeed be a common result of the latent heat of crystallization[4] as well as viscous[5,6] and frictional[7] heating in areas of strain localization. Here we present field and experimental observations of magma vesiculation and fragmentation resulting from heating (rather than decompression). Textural analysis of volcanic ash from Santiaguito volcano in Guatemala reveals the presence of chemically heterogeneous filaments hosting micrometre-scale vesicles. The textures mirror those developed by disequilibrium melting induced via rapid heating during fault friction experiments, demonstrating that friction can generate sufficient heat to induce melting and vesiculation of hydrated silicic magma. Consideration of the experimentally determined temperature and pressure dependence of water solubility in magma reveals that, for many ascent paths, exsolution may be more efficiently achieved by heating than by decompression. We conclude that the thermal path experienced by magma during ascent strongly controls degassing, vesiculation, magma strength and the effusive–explosive transition in volcanic eruptions.

Volcanic eruptions result from magma buoyancy, largely powered by volatile exsolution. In standard models of magma ascent this exsolution is triggered by decompression[8,9]. Upon ascent, gas bubbles (vesicles) expand and pressure build-up may precipitate fragmentation and explosive eruption[1]. Yet the solubility, which sets the thermodynamic driving force for saturation and vesiculation in a volatile component has long been known to be a function of temperature as well[10]. Thus temperature changes may also generate magma vesiculation. Despite this, to our knowledge, no models of volcanic eruptions have explored the role of temperature in generating magmatic vesicularity.

The thermal evolution of magma in volcanic conduits has received increased attention in recent years. First, petrological studies have demonstrated that crystallizing magmas can heat up considerably (up to about 100 °C) owing to the latent heat liberated[4]—a process acting across the entire magmatic column. Second, zones in which magma undergoes strain localization during ascent also exhibit evidence of considerable heating (up to about 250 °C) resulting from viscous energy dissipation[5,6,11,12]. Third, the discovery of pseudotachylytes (caused by frictional melting during faulting) in erupted dome rocks[13] and at the margin of lava spines[7] indicates that fault friction can be an important contributor to the thermal budget of magma (locally up to about 1,000 °C), thus strongly affecting volcanic eruption dynamics[14].

Evidence is mounting that magma ascent may often be controlled by strain localization near conduit margins[15]. Such strain localization in magmas has been proposed as a scenario leading to failure and potentially serving as a trigger for explosive eruptions[16,17]. Careful examination of shallow volcanic conduit structures lends support to these proposals[18]. Magmatic conduits or dykes are relatively narrow (tens of centimetres to a few metres) at depths of a few kilometres[19], so regions of strain localization may represent an important mass fraction of ascending magma. At shallow depths, where conduits can be wider (metres to a few tens of metres), areas of strain localization may not appear to be inevitable, yet the observation that shallow magma bodies are heavily fractured[20], and the influence of such fractures on surficial magma behaviour[21] suggest that strain localization and its associated heat may play a large part throughout the length of the magmatic column.

Estimates of magma ascent rates vary widely. In general, explosive eruptions have been associated with high ascent rates, reaching up to a few metres per second before fragmentation[9]. During such rapid ascent, magma decompresses (one metre per second corresponds to a decompression of 0.02 MPa per second) and simultaneously heat is generated in all areas where strain is localized, either by fault friction[14] or viscous dissipation[12]. The material record of such heat may or may not be documented in the products of the subsequent volcanic explosions. The mineralogical assemblage can often preserve information related to such heating[7,13], but if sufficient time passes then the assemblage will recover in response to the mean temperature and pressure conditions and evidence of fluctuations may be lost. The glassy state itself does not provide direct information from above the glass transition temperature, yet, indirectly, evidence of energy dissipation has been inferred from the morphology of the porous network preserved in glassy volcanic products[5,6]. The difficulty of preservation of evidence of heating in ascending magma, or of the temperature history, is probably a major reason for its neglect in eruption models.

Temperature and pressure both affect the solubility of water[22–24] (the dominant volatile component of volcanic activity) in magma. For a calc-alkaline rhyolitic melt, the temperature- and pressure-dependence of water solubility can be estimated by[24]:

$$(H_2O)_{total} = \frac{354.94P^{0.5} + 9.623P - 1.5223P^{1.5}}{T} + 0.0012439P^{1.5} \quad (1)$$

where $(H_2O)_{total}$ is the total dissolved H_2O content (in weight per cent, wt%), T is temperature (in K), and P is pressure (in MPa). Figure 1a shows that owing to the strongly retrograde nature of the H_2O solubility curve at low pressures, an increase in temperature is a driving force

[1]Department of Earth, Ocean and Ecological Sciences, University of Liverpool, Liverpool L69 3GP, UK. [2]Department of Earth and Environmental Sciences, Ludwig Maximilian University of Munich, Theresienstrasse 41/III, 80333 Munich, Germany. [3]Department of Geosciences, Boise State University, Boise, Idaho, USA. [4]Geological Sciences, University of Canterbury, Private Bag 4800, 8140 Christchurch, New Zealand. [5]Department of Mineral Sciences, Smithsonian Institution, Washington, District of Columbia, USA. [6]Instituto Nacional de Sismologia, Vulcanologia, Meteorologia, e Hydrologia (INSIVUMEH), 7a Avenue 14-57, Zone 13, Guatemala City, Guatemala.

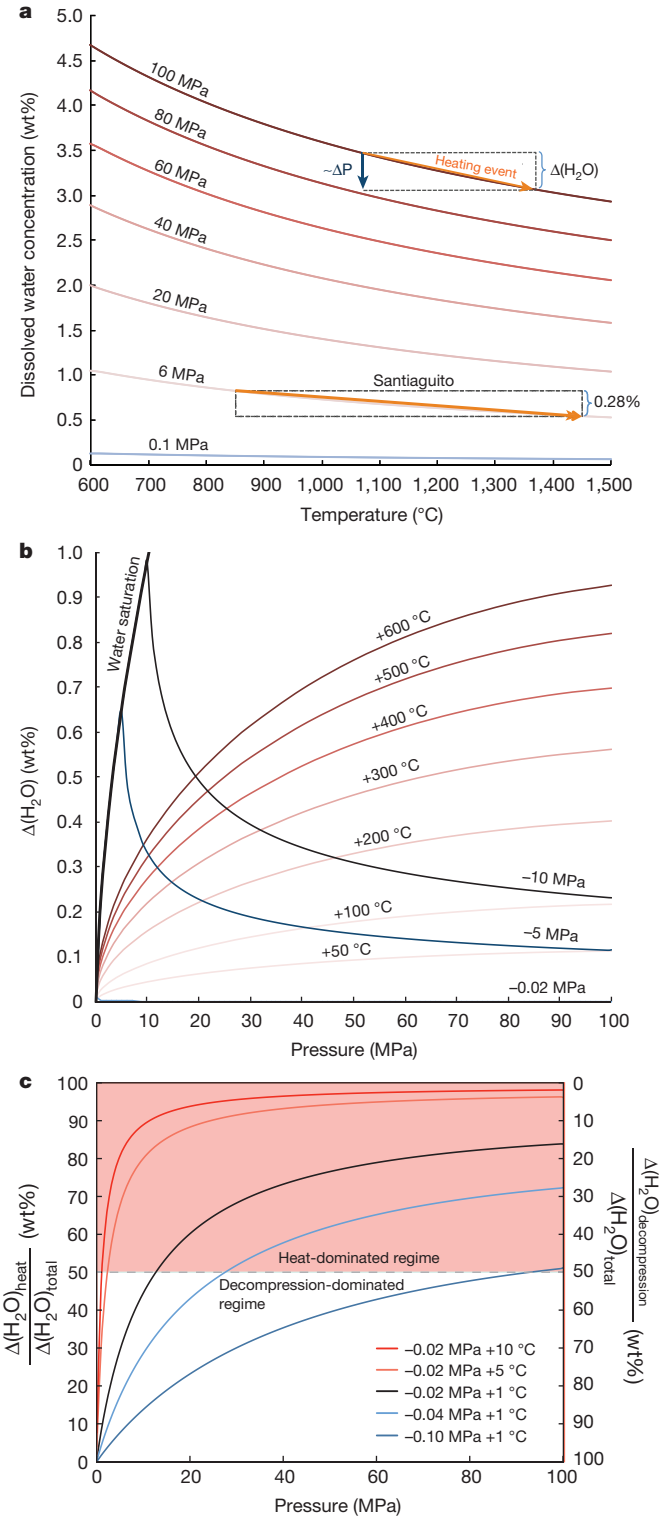

Figure 1 | Water concentration in rhyolitic magmas. **a**, Thermobarometric limits on water concentration[24] show that the heat induced by mechanical work (orange arrows) during magma ascent causes a decrease in water solubility, $\Delta(H_2O)$. This decrease in concentration may be related to an equivalent decompression, $\sim\Delta P$. At Santiaguito, thermal input of, for example, ~600 °C owing to short-lived faulting events may reduce water solubility by 0.28 wt%. **b**, Water exsolution, $\Delta(H_2O)$, driven by thermal input (red curves) versus decompression events (blue curves) for an ascending magma at a nominal temperature of 850 °C. These heating and decompression events are computed as a function of melt pressure at which the event initiates in the magmatic column. **c**, Fraction of the total water concentration exsolved from the action of heat (left *y* axis), versus that of decompression (right *y* axis) for different decompression and heating events. The data shows that thermal input (which acts on a timescale of seconds) generally induces more water exsolution than decompression.

for vesiculation in this pressure range. This temperature dependence is clearly large enough to have a substantial effect on water saturation during magma ascent in conduits.

We analysed the potential magnitude of water exsolution ΔH_2O that is due to (1) decompression and (2) heating at a magmatic temperature of 850 °C (Fig. 1b). The comparison of the individual effects of decompression versus heating yields striking results. We found that events that heat magma by hundreds of degrees, as described above, strongly drive substantial exsolution and vesiculation. For an ascent rate of one metre per second (that is, 0.02 MPa per second, which is capable of triggering explosive events), 1 K of heating has the potential to generate more water exsolution than 0.02 MPa of decompression from initial pressures greater than 13 MPa (Fig. 1c), and further heating can be the main driving force for vesiculation. Expressing it in a different way, a decompression event exceeding 0.1 MPa (>5 m of ascent) would be required to exsolve more water than that exsolved by 1 °C of heating. We therefore conclude from this analysis that the thermal path of decompressing magma can greatly influence volatile exsolution. It is thus easy to envisage scenarios of heating-dominated or 'thermal' vesiculation during magma ascent at moderate pressures, and below we provide evidence to support the assertion that such thermal exsolution is also dominant during strain localization in magma at shallower depths.

We have examined eruptive products at the Santiaguito dome complex. The active Caliente lava dome offers one of the most spectacular displays of cyclic, piston-like eruptive activity ever recorded, often climaxing in gas-and-ash explosions along concentric fractures[21,25,26] (Fig. 2a). Proximal monitoring of this dome has revealed a regular (~26 min) periodicity in ground inflation–deflation cycles[27]. At the expansion maxima, the propagation of arcuate faults across the dome's surface is observed and the dome's centre thrusts upward and collapses back, followed by dome deflation[21]. Gas-and-ash explosions occur episodically along the faults, coincident with very-long-period seismic events, which have been interpreted to be associated with gas flow in fractures at the inflation maximum (Fig. 2b)[27]. In the analysis that follows, the rates of inflation and deflation during ash release and the magnitude and rate of slip are of central importance. Ash ejection occurs only during the fastest inflation–deflation cycles (Fig. 2b)[27]. In these cases, the arcuate faults undergo a metre of uplift and collapse within one second, corresponding to a slip rate of $<2\ m\ s^{-1}$ (ref. 21). Importantly, these lava dome dynamics leave striation and slickensides (frictional marks) on the blocks forming the dome carapace.

Textural examination of volcanic ash collected upon deposition in November 2012 and November 2014 provides several examples of the material consequences of such frictional processes (Extended Data Figs 1–4). The interstitial glass phase reveals a juxtaposition of chemically distinct mingled filaments with different shades of grey on back-scattered electron (BSE) images obtained by scanning electron microscopy (SEM; Fig. 2c; Extended Data Figs 3 and 4). The contacts between the light- and darker-toned filaments are diffuse and fluid (unlike crystals with sharp and angular boundaries). The very fine nature of these filaments and the diffuse boundaries prevent us from accurately using standard geochemical analysis techniques, but the greyscale values observed (which reflect the atomic number and thus chemical variations within and between phases) provide clear evidence of chemical heterogeneity (Fig. 2c; Extended Data Fig. 4). These melt phases have evidently mingled with the original interstitial melt on timescales insufficient for homogenization, presumably immediately before the fragmentation and eruption that locked in these dynamic features.

The mingling textures exhibited by the Caliente ash mirror those of protomelts resulting from selective melting of individual

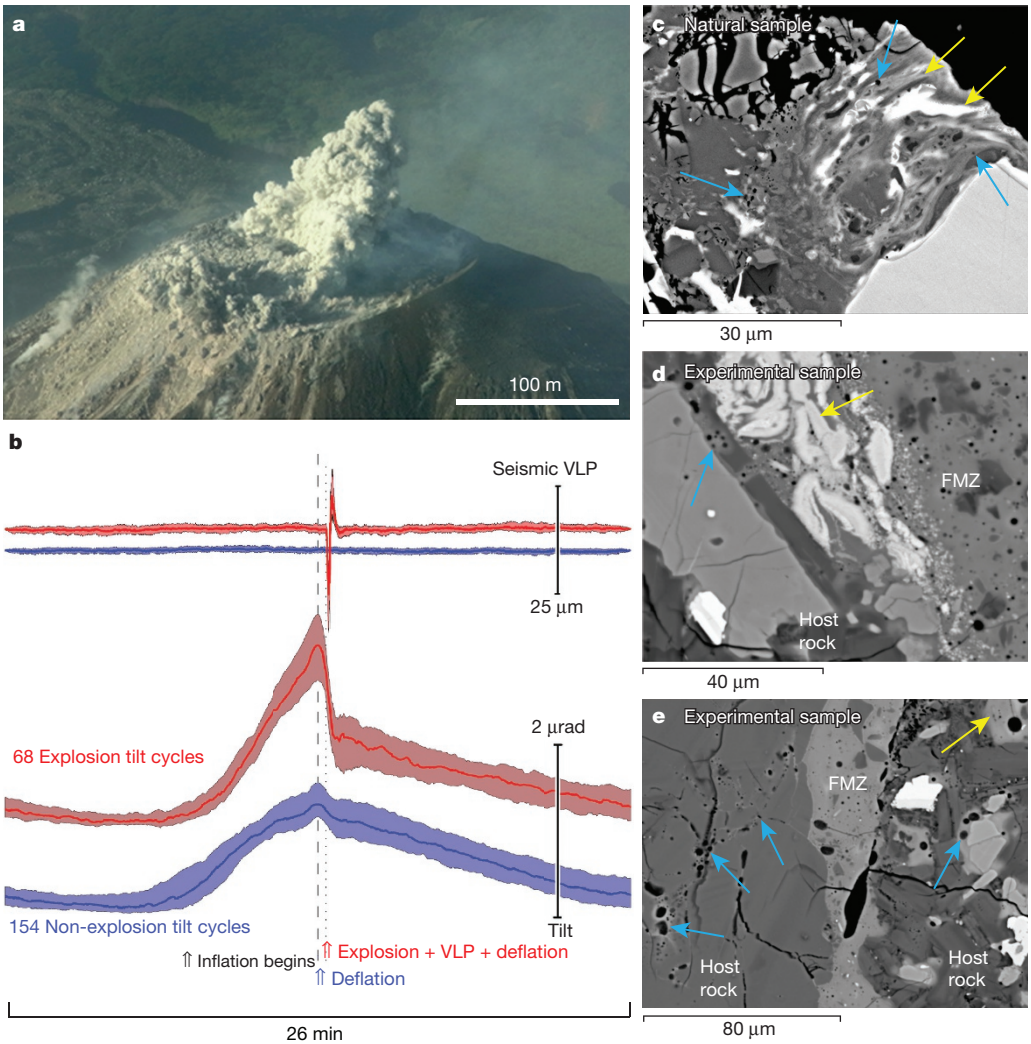

Figure 2 | Explosive eruptions caused by superheated vesiculation. a, Gas-and-ash explosion occurring along an arcuate fault on 10 November 2012 at Caliente dome, Santiaguito. **b**, Seismic signals (upper) and tilt data (lower) for explosive (red) and non-explosive (blue) inflation–deflation cycles associated with piston-like dynamics at Santiaguito[27]. The solid lines display the average of the 26-min cycles over the five-day-long data set, whereas the shaded areas exhibit the spread in the data. Gas-and-ash explosion cycles differ markedly from non-explosive cycles and are characterized by faster and stronger inflation or deflation as well as very-long-period (VLP) seismic events. Note that the exact timing of the seismic and tilt signals may be offset slightly. **c**, BSE image showing heterogeneous protomelt filaments (yellow arrows) with different greyscale values (a proxy for chemical composition; darker grey indicates lighter elements and vice versa) extruded from crystals present in a volcanic ash particle sampled on 12 November 2012; some protomelts host vesicles (blue arrows). **d**, BSE image showing the shearing of protomelts near the main frictional melt zone (FMZ), produced experimentally by fault slip. **e**, BSE image showing vesiculation of the interstitial melt near the experimental fault zone, caused by high local temperature.

crystals that have been observed in the products of frictional melting experiments[28,29]. Such experiments involve an extremely rapid heating rate (more than tens to hundreds of degrees Celsius per second) and therefore highly disequilibrium melting induced by fault friction[28–30]. We propose here that the Caliente ash samples contain volcanic pseudotachylyte; evidence of the syn-eruptive operation of frictional heating sufficient to generate melting in the piston-like events at Caliente dome. Notably, the protomelts present in the ash contain vesicles (as indicated by blue arrows on Fig. 2c). The crystalline phases present are anhydrous and thus cannot serve as a source of water for vesiculation, so we suggest that vesiculation took place in the interstitial melt. If so, these frictional melts contain clear evidence of thermal vesiculation in volcanic products.

As an experimental demonstration of the feasibility of thermal vesiculation, we have performed fault friction experiments under conditions designed to simulate the piston-like gas-and-ash explosion events at Caliente[21]. During the experiments the flat ends of two hollow, cylindrical cores of a Caliente dome rock were pushed together at an applied normal stress of 6 MPa (representative of the depth of tilt and seismic sources[27]) and one core was rotated (against the other) at an equivalent velocity of 1 m s^{-1} (see Methods and Extended Data Fig. 5). Friction experiments on magmas have shown that under such conditions frictional melting takes place within as little as about 10 cm of slip[13,14,28] confirming the feasibility of this process.

As noted above, microscopic inspection of the fault products experimentally generated in the Caliente dome rock reveals the presence of multiple, chemically heterogeneous melt filaments extruded from crystals adjacent to the fault zones (Fig. 2d; Extended Data Fig. 6). In addition, the interstitial glass of the host rock in the first 0.3–0.4 mm near the fault zone has partially vesiculated (Fig. 2e; Extended Data Fig. 7). To ensure that vesiculation resulted from substantial heat near the fault zone, we have tested the stability of dissolved water in this dome rock at background magmatic temperature by subjecting two small cores to 850 °C for 30 min and 15 h, respectively. We observe that no water exsolved to form vesicles, even after a 15-h dwell (Extended Data Fig. 8). We conclude from these experiments that both the generation of crystal protomelts and the surrounding vesiculation result directly from the frictional work converted to substantial heat during faulting events, and are not due to residence at magmatic temperature. From the similarity of these experimental products of frictional melting to the natural samples of Caliente (described above) we deduce that the cyclic phenomena observed during dome extrusion and explosions at Caliente occur in the presence of strain localization, accompanied by thermal vesiculation.

The occurrence of superheated vesiculation at Caliente can be assessed by modelling the conversion of mechanical work to heat (ΔT) during friction, using[31]:

$$\Delta T = \frac{\mu \sigma_n V \sqrt{t}}{\rho C_p \sqrt{\pi k}} \quad (2)$$

Using Byerlee's friction coefficient μ of 0.85 (at static conditions), a normal stress σ_n of 6 MPa (ref. 27), a slip velocity V of 1 m s^{-1} for a duration t of 0.5 s (ref. 21), a density ρ of 2,630 kg m^{-3} (determined by helium pycnometry), a specific heat capacity C_p of 900 J kg^{-1} K^{-1}, and a thermal diffusivity k of 10^{-6} m^2 s^{-1}, uplift of the dome would generate a local temperature increase of 860 °C along the arcuate faults.

Given that the magma already resides at ~850 °C (ref. 32), and that experimental work has shown that only moderate temperature increase occurs once frictional melt lubricates a slip zone[13,14,28], the temperature would not be expected to greatly exceed the melting temperatures of the main rock-forming minerals in the Caliente lava (labradorite and enstatite, which melt at >1,300 °C and >1,400 °C, respectively[30]). This magnitude of heating would induce water exsolution from the melt in zones of strain localization. Owing to the current eruptive cycles and outgassing activity at Caliente, we consider the system to be open to an extent that allows for exsolution of any oversaturated volatile fraction; thus a total of 0.83 wt% would be expected to remain in the magma at the point of fragmentation at 6 MPa (Fig. 1a). Heating of ~550–860 °C would induce a dramatic oversaturation in water of 0.26–0.35 wt%. Faulting, creation of new surface area, and forced convection during frictional melting would all serve to minimize effective diffusion path lengths and enhance the completion of water exsolution. With such overheating, and thus heightened H_2O diffusivity, the kinetic limitation to vesiculation (nucleation and growth) should also be easily overcome, promoting foaming. At a depth of about 300 m such vesiculation would, in turn, reduce the strength of magma and thereby trigger fragmentation[33]. We therefore conclude that vesiculation can be induced by rapid heating in the conduit.

Water is central to magma ascent dynamics and its contribution to magmatic and volcanic processes results from a combination of both pressure and temperature. Decompression is inevitable and acts throughout magma ascent. Here we argue that heating via both crystallization and shearing processes are equally inevitable. More specifically, the magnitude of viscous and frictional heating may be prodigious, and thus exert a primary control on volatile exsolution. At the rates and magnitudes of heating discussed here, the solubility of water in a melt should be affected before heat loss by thermal conductivity to the cooler surroundings—whether in the core of the magmatic column (where further water may exsolve) or in the country rock—could serve to counteract local heating. Heating during magma ascent deserves adequate consideration in conduit transport and eruption models.

The idea that temperature may dominate the dynamics of water saturation and vesiculation during magma transport in volcanic conduits means that the thermal path experienced by magmas during ascent need to be better constrained. A thorough reassessment of strain localization across deep dykes and shallow conduits should lead to the quantification of shear heating during magma transport. In light of the demonstration that heating may supercede decompression as a driving force for degassing, we call for this concept to be included in the simulation and analysis of magma ascent and eruption.

Online Content Methods, along with any additional Extended Data display items and Source Data, are available in the online version of the paper; references unique to these sections appear only in the online paper.

Received 4 January; accepted 6 October 2015.

1. Sahagian, D. Magma fragmentation in eruptions. *Nature* **402,** 589 (1999).
2. Vasseur, J., Wadsworth, F. B., Lavallée, Y., Hess, K.-U. & Dingwell, D. B. Volcanic sintering: timescales of viscous densification and strength recovery. *Geophys. Res. Lett.* **40,** 5658–5664 (2013).
3. Dingwell, D. B. Volcanic dilemma: flow or blow? *Science* **273,** 1054–1055 (1996).
4. Blundy, J., Cashman, K. & Humphreys, M. Magma heating by decompression-driven crystallization beneath andesite volcanoes. *Nature* **443,** 76–80 (2006).
5. Rosi, M., Landi, P., Polacci, M., Di Muro, A. & Zandomeneghi, D. Role of conduit shear on ascent of the crystal-rich magma feeding the 800-year-BP Plinian eruption of Quilotoa Volcano (Ecuador). *Bull. Volcanol.* **66,** 307–321 (2004).
6. Wright, H. M. N. & Weinberg, R. F. Strain localization in vesicular magma: implications for rheology and fragmentation. *Geology* **37,** 1023–1026 (2009).
7. Kendrick, J. E. *et al.* Extreme frictional processes in the volcanic conduit of Mount St. Helens (USA) during the 2004–2008 eruption. *J. Struct. Geol.* **38,** 61–76 (2012).
8. Martel, C. & Schmidt, B. C. Decompression experiments as an insight into ascent rates of silicic magmas. *Contrib. Mineral. Petrol.* **144,** 397–415 (2003).
9. Proussevitch, A. A. & Sahagian, D. L. Dynamics and energetics of bubble growth in magmas: Analytical formulation and numerical modeling. *J. Geophys. Res. Solid Earth* **103,** 18223–18251 (1998).
10. Ghiorso, M. S. & Sack, R. O. Chemical mass-transfer in magmatic processes. 4. A revised and internally consistent thermodynamic model for the interpolation and extrapolation of liquid-solid equilibria in magmatic systems at elevated temperatures and pressures. *Contrib. Mineral. Petrol.* **119,** 197–212 (1995).
11. Hess, K. U., Cordonnier, B., Lavallée, Y. & Dingwell, D. B. Viscous heating in rhyolite: an in situ determination. *Earth Planet. Sci. Lett.* **275,** 121–126 (2008).
12. Mastin, L. G. The controlling effect of viscous dissipation on magma flow in silicic conduits. *J. Volcanol. Geotherm. Res.* **143,** 17–28 (2005).
13. Kendrick, J. E. *et al.* Seismogenic frictional melting in the magmatic column. *Solid Earth* **5,** 199–208 (2014).
14. Kendrick, J. E. *et al.* Volcanic drumbeat seismicity caused by stick-slip motion and magmatic frictional melting. *Nature Geosci.* **7,** 438–442 (2014).
15. Lavallée, Y., Hess, K.-U., Cordonnier, B. & Dingwell, D. B. Non-Newtonian rheological law for highly crystalline dome lavas. *Geology* **35,** 843–846 (2007).
16. Gonnermann, H. M. & Manga, M. Explosive volcanism may not be an inevitable consequence of magma fragmentation. *Nature* **426,** 432–435 (2003).
17. Papale, P. Strain-induced magma fragmentation in explosive eruptions. *Nature* **397,** 425–428 (1999).
18. Tuffen, H., Dingwell, D. B. & Pinkerton, H. Repeated fracture and healing of silicic magma generate flow banding and earthquakes? *Geology* **31,** 1089–1092 (2003).
19. Noguchi, S., Toramaru, A. & Nakada, S. Groundmass crystallization in dacite dykes taken in Unzen scientific drilling project (USDP-4). *J. Volcanol. Geotherm. Res.* **175,** 71–81 (2008).
20. Stasiuk, M. V. *et al.* Degassing during magma ascent in the Mule Creek vent (USA). *Bull. Volcanol.* **58,** 117–130 (1996).
21. Johnson, J. B., Lees, J. M., Gerst, A., Sahagian, D. & Varley, N. Long-period earthquakes and co-eruptive dome inflation seen with particle image velocimetry. *Nature* **456,** 377–381 (2008).
22. Holtz, F., Behrens, H., Dingwell, D. B. & Johannes, W. H_2O solubility in haplogranitic melts—compositional, pressure and temperature-dependence. *Am. Mineral.* **80,** 94–108 (1995).
23. Ryan, A. G., Russell, J. K., Nichols, A. R. L., Hess, K.-U. & Porritt, L. A. Experiments and models on H_2O retrograde solubility in volcanic systems. *Am. Mineral.* **100,** 774–786 (2015).
24. Liu, Y., Zhang, Y. X. & Behrens, H. Solubility of H_2O in rhyolitic melts at low pressures and a new empirical model for mixed H_2O–CO_2 solubility in rhyolitic melts. *J. Volcanol. Geotherm. Res.* **143,** 219–235 (2005).
25. Holland, A. S. P., Watson, I. M., Phillips, J. C., Caricchi, L. & Dalton, M. P. Degassing processes during lava dome growth: insights from Santiaguito lava dome, Guatemala. *J. Volcanol. Geotherm. Res.* **202,** 153–166 (2011).
26. Scharff, L., Hort, M. & Gerst, A. The dynamics of the dome at Santiaguito volcano, Guatemala. *Geophys. J. Int.* **197,** 1–17 (2014).
27. Johnson, J. B., Lyons, J. J., Andrews, B. J. & Lees, J. M. Explosive dome eruptions modulated by periodic gas-driven inflation. *Geophys. Res. Lett.* **41,** 6689–6697 (2014).
28. Hornby, A. J. *et al.* Spine growth and seismogenic faulting at Mt. Unzen, Japan. *J. Geophys. Res. Solid Earth* **120,** 4034–4054 (2015).
29. Lin, A. M. & Shimamoto, T. Selective melting processes as inferred from experimentally generated pseudotachylytes. *J. Asian Earth Sci.* **16,** 533–545 (1998).
30. Spray, J. G. in *Annual Review of Earth and Planetary Sciences* Vol. 38 (ed. Jeanloz, R. F. K. H.) 221–254 (2010).
31. Carslaw, H. S. & Jaeger, J. C. *Conduction of Heat in Solids* 2nd edn (Oxford Univ. Press, 1959).
32. Harris, A. J. L. & Flynn, L. P. The thermal stealth flows of Santiaguito dome, Guatemala: implications for the cooling and emplacement of dacitic block-lava flows. *Geol. Soc. Am. Bull.* **114,** 533–546 (2002).
33. Zhang, Y. X. A criterion for the fragmentation of bubbly magma based on brittle failure theory. *Nature* **402,** 648–650 (1999).

Acknowledgements We thank A. Pineda, the staff at the National Institute for Seismology, Vulcanology, Meteorology and Hydrology of Guatemala (INSIVUMEH) and the Policia Nacional Civil de Guatemala for support with the field campaign. This work was supported by a European Research Council Starting Grant to Y.L. on 'Strain Localisation in Magmas' (SLiM, grant number 306488) and an Advanced Grant to D.B.D. on 'Explosive volcanism in the Earth system' (EVOKES, grant number 247076). J.B.J acknowledges the National Science Foundation EAR-grant number 1151662. This work was partially funded by the European Union's seventh programme for research, technological development, and demonstration under grant agreement 282759 (VUELCO), and by an AXA grant 'Risk from Volcanic Ash in the Earth System'. We are grateful to K. Genereau and L. Mastin for constructive reviews.

Author Contributions Y.L., J.E.K., F.W.v.A., A.J.H., F.B.W., B.J.A., B.M.K. and D.B.D. conceptualized the model. G.C. facilitated fieldwork and supported data analysis. Y.L., C.C., F.B.W., A.J.H., B.M.K. and E.R. performed fieldwork, collected samples and Y.L., F.W.v.A., A.J.H. and J.E.K. analysed the ash. A.J.H., J.E.K. and Y.L. performed the experiments. J.B.J. performed the geophysical analysis. All authors contributed to the manuscript.

Author Information Reprints and permissions information is available at www.nature.com/reprints. The authors declare no competing financial interests. Readers are welcome to comment on the online version of the paper. Correspondence and requests for materials should be addressed to Y.L. (yan.lavallee@liverpool.ac.uk).

METHODS

Volcanic ash sampling and analysis. The ash samples were collected after each explosion from a location (14° 44′ 35.11″ N, 91° 33′ 40.69″ W) approximately 275 m east-northeast from the active Caliente vent. The ash was collected by spreading a clean, 1.4 m × 1.4 m synthetic sheet. We used a paintbrush to carefully brush deposited ash into sample bags. The sheets were thoroughly cleaned after each sample collection and laid out to collect the ash of subsequent events. Owing to the proximity of the sampling location, we are very confident of the source and timing of the ash employed in this study.

The grain size of the sampled volcanic ash was measured using a laser diffraction particle size analyser from Coulter. The density was determined on 25-mm-diameter and 50-mm-long rock cores using a 100-cm^3 helium pycnometer from Micromeritics.

SEM analysis and energy-dispersive X-ray spectroscopy. Geochemical mapping across the natural samples and the experimental products was conducted in a Phillips XL 30 SEM using BSE and energy-dispersive X-ray spectroscopy (EDS) run on the Oxford Instruments INCA software. BSE images provide an excellent means of identifying frictional melting textures, because the grey value of each phase relates to the atomic number, or the density of major elements representing the geochemical composition[34]. A dense phase consisting of heavy elements elastically reflects more electrons and thus shows up in light grey on a BSE image; conversely, an elementally light phase shows up in dark grey.

EDS was used to map the chemical concentration of major elements present in the different phases observed by BSE imaging. The EDS system allows mapping of the distribution of these elements across the main phases. We used an electron beam of 5.5 μm at 20 keV and 8 nA. For the purpose of this study, we monitored the distribution of Si, Mg, Fe, Ti, Na and Al. Comparison of BSE and EDS images verify that the filaments have different chemical compositions.

Electron probe micro-analysis. Geochemical analysis of the phases present in the natural samples and the experimental products was performed in a CAMECA SX 100 Electron Probe Micro Analyser at the Ludwig Maximilian University of Munich in Germany. Probing of the glass and mineral phases was done using a focused electron beam of 15 keV and 20 nA (Extended Data Fig. 6). Note that because we used a focused beam on glass, the measured concentrations of the alkalis, namely Na and K, are reduced by some 0.1–0.3 wt% from what is likely to be present; however, the filaments were too thin to be measured with a defocused beam, which would yield higher inaccuracy. Despite this, the results reveal the chemical distinction between the different phases.

In Extended Data Fig. 6, we present the chemical composition of only the primary minerals and glass, and the protomelts and main frictional melt from the experiments, because the phases were large enough to be analysed. In the natural ash, the filaments are rarely larger than 1 μm (see Extended Data Figs 2–4) and so electron microprobe analysis was impracticable without a large degree of contamination from surrounding phases; hence, we used the greyscale in BSE images as well as EDS elemental maps to verify the occurrence of the same processes as observed in the experimental samples.

Fault slip experiments. The friction experiment was conducted in a low- to high-velocity rotary shear apparatus at the University of Liverpool, designed by T. Shimamoto and built by Marui, Japan. The experiment was conducted on two hollow, cylindrical samples with outer and inner diameters of 24.99 mm and 15.86 mm, respectively (Extended Data Fig. 5). The samples were axially loaded using an air actuator at a normal stress of 6.0 MPa, as constrained by the depth of seismicity, and slip was applied on one rotating sample via a servo motor operated at 1,200 rotations per minute, to induce an equivalent slip rate of 1 m s^{-1}, while the other sample was held stationary (see Hirose and Shimamoto[35] for further detail of apparatus and method). After the test, the sample was cut and a thin section was prepared.

Testing the stability of volatiles in the dome rock at eruptive temperature. We conducted complementary experiments to test the ability of the rock to vesiculate at high temperature to ensure that foaming observed in the friction experiments results from the very high temperatures achieved during fault slip, instead of simply because the rock used contains a concentration of water (quenched-in at high pressure) higher than that which is stable at atmospheric pressure. For this purpose, two small 8 mm × 8 mm cylindrical samples were heated to a magmatic temperature of 850 °C and one was allowed to dwell for 30 min while the other was allowed to dwell for 15 h. After the experiment, the samples were cut, polished and carbon-coated for SEM analysis.

34. Petruk, W. *Applied Mineralogy in the Mining Industry* 1st edn, 268 (Elsevier, 1990).
35. Hirose, T. & Shimamoto, T. Growth of molten zone as a mechanism of slip weakening of simulated faults in gabbro during frictional melting. *J. Geophys. Res. Solid Earth* **110,** http://dx.doi.org/10.1029/2004JB003207 (2005).

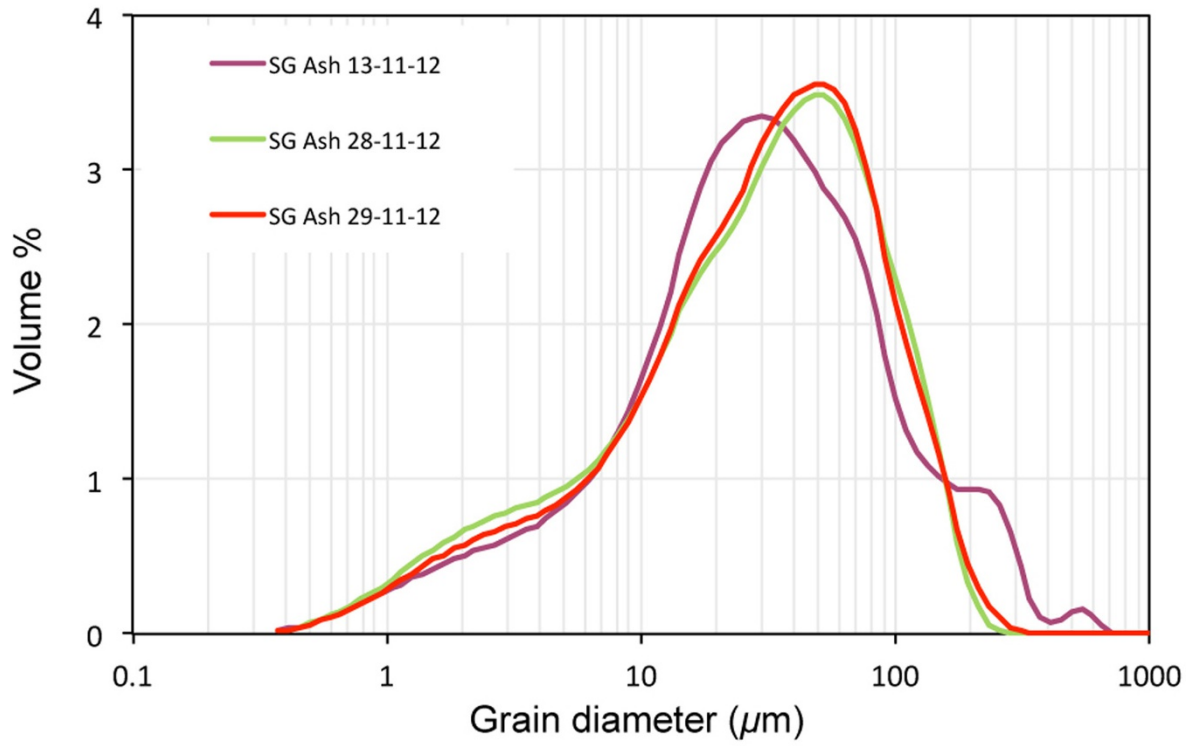

Extended Data Figure 1 | Grain size distribution of three volcanic ash samples collected during November 2012. At this proximal sampling location (275 m from the vent), most of the ash recovered is below 200 μm in size and the dominant grain size peaks at around 50 μm. The measurements were made using a laser diffraction particle size analyser from Coulter.

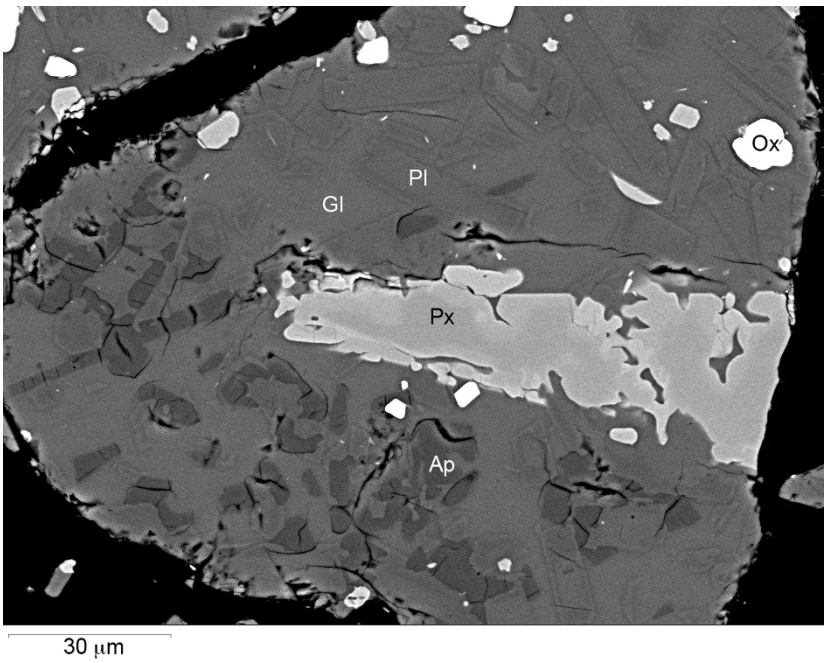

Extended Data Figure 2 | BSE image showing the different phases present in the eruptive products at Caliente. The dome rocks and the volcanic ash samples contain primarily plagioclase (Pl, dark grey), pyroxene (Px, light grey), iron oxides (Ox, white), apatite (Ap, very dark grey) and interstitial glass (Gl, dark grey). Note the absence of vesicles (black, rounded pores) in this dense ash fragment, which contains less than 2% pore space. Despite the fact that there are no vesicles in this ash particle, we note that the edge of the iron oxides and pyroxene crystals are not straight, but rather crenulated and somewhat diffuse.

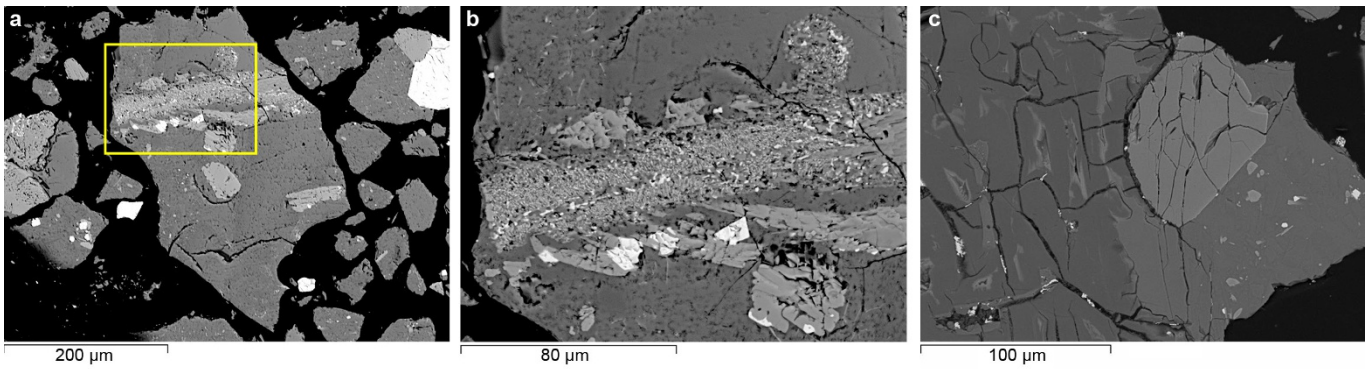

Extended Data Figure 3 | BSE images showing heterogeneous melt filaments present in volcanic ash erupted at Caliente. a, **b**, 13 November 2012; **c**, 26 November 2014. The yellow box in **a** defines the region of interest displayed in **b**. Evidence for high thermal input is best represented by the occurrence of frictional melting. The characteristic texture of frictional melting has been noted in a number of volcanic ash particles and from several eruptions (the main text refers to ash from 10 November 2012). The textures associated with frictional melting preserved in the ash erupted on 13 November 2012 and 26 November 2014, suggest that this dynamic of strain localization in magma was active for at least two years.

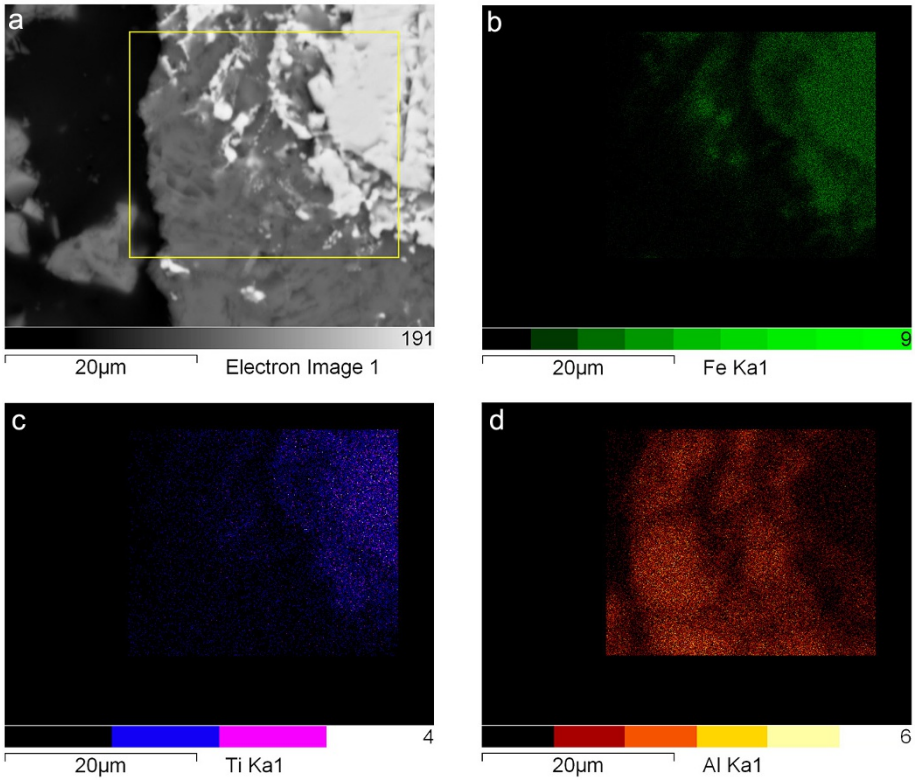

Extended Data Figure 4 | EDS images showing the heterogeneous concentration of various elements in the melt filaments. a, BSE image showing the area mapped by EDS. EDS maps show the distribution of Fe (**b**, in green), Ti (**c**, in blue), and Al (**d**, in red). Colour-scale values represent X-ray counts per pixel for each energy band in the line type Ka1. During frictional melting of andesite and dacite, selective melting tends to affect the iron-titanium oxides more readily than silicate mineral phases owing to their lower fusion temperature[30].

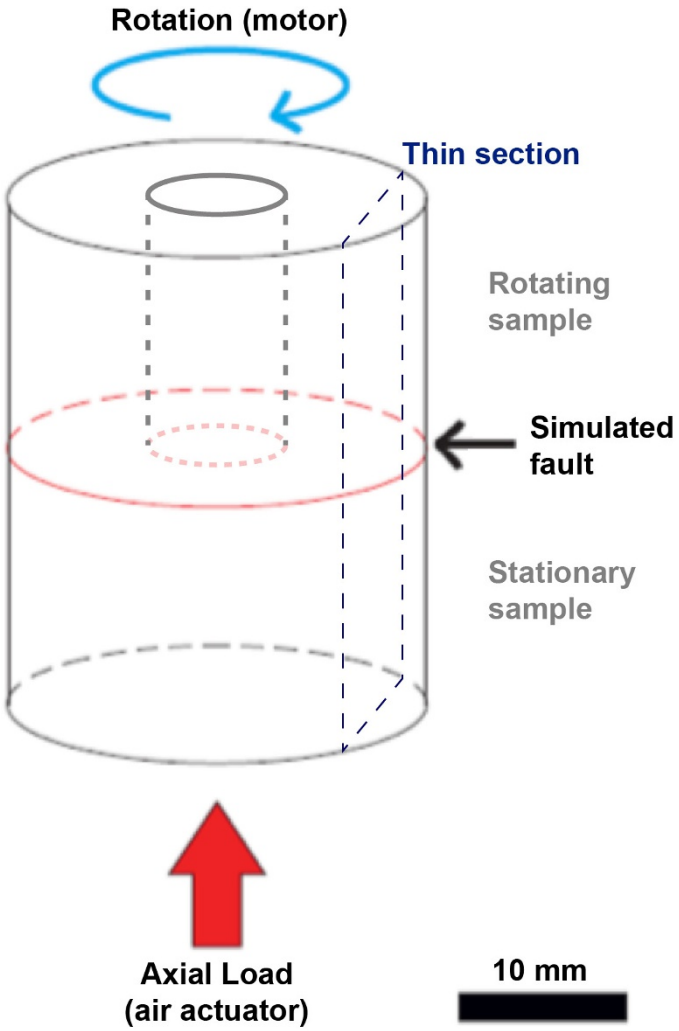

Extended Data Figure 5 | Sample assembly setup during rotary shear experiments. The sketch also highlights the area sliced for thin-section preparation.

a

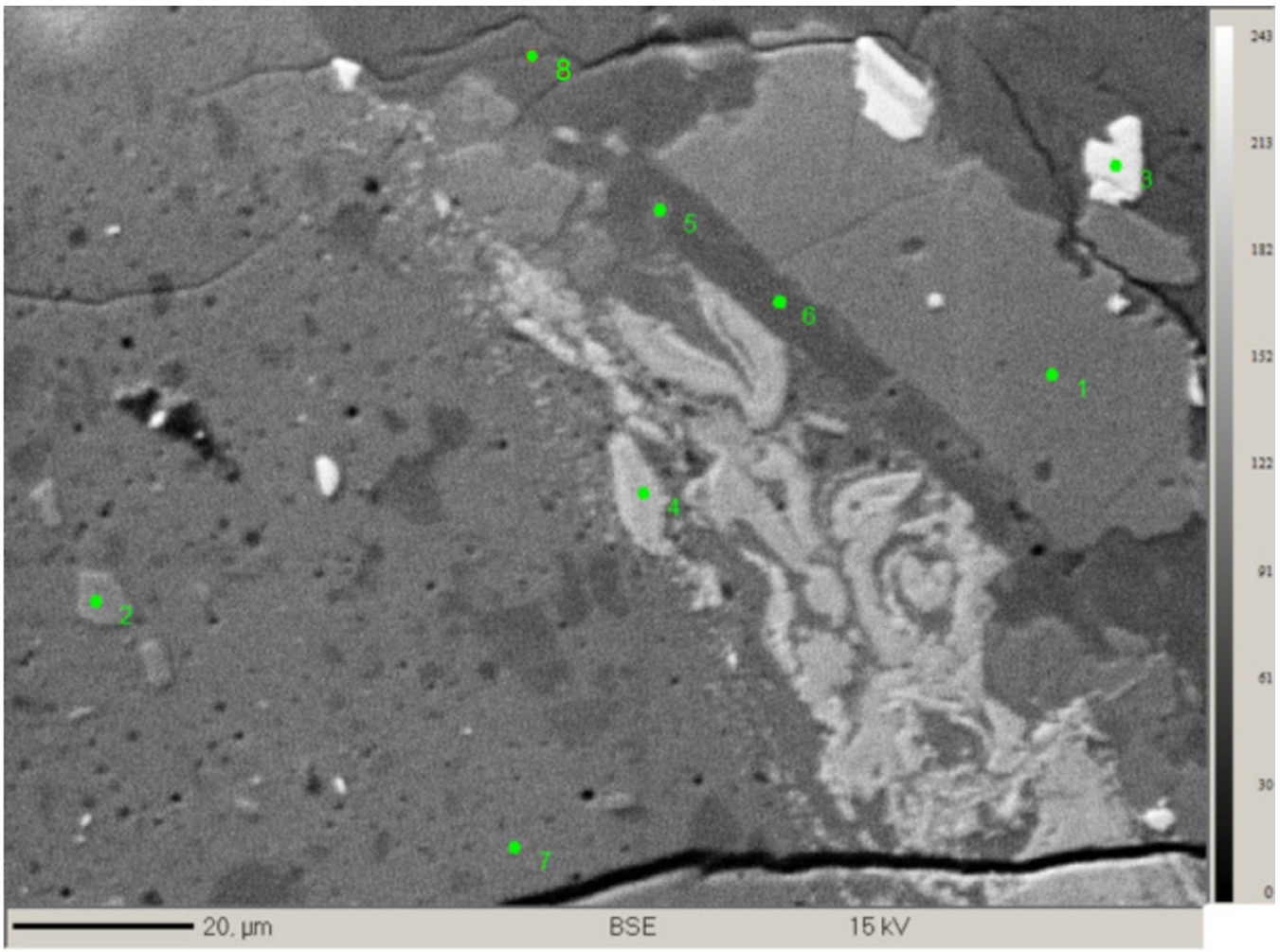

b

	#1	#2	#3	#4	#5	#6	#7	#8
Oxides	Clinopyroxene	Orthopyroxene	Fe-Oxide	Protomelt	Protomelt	Plagioclase	Frictional melt	Plagioclase
SiO_2	51.17	52.62	1.30	24.50	54.91	53.70	53.28	56.59
Al_2O_3	2.36	0.93	1.26	2.23	15.22	28.30	16.51	25.62
Na_2O	0.36	0.14	0.00	0.67	2.90	4.81	3.47	5.48
K_2O	0.02	0.03	0.17	0.40	0.69	0.25	0.94	0.73
MgO	15.32	18.06	0.59	7.75	7.98	0.09	6.76	0.64
CaO	16.66	6.32	0.31	0.85	8.37	11.43	7.37	9.15
TiO_2	0.98	0.43	9.43	0.18	0.40	0.04	1.00	0.04
FeO	12.55	20.75	-	-	9.07	1.37	10.27	1.66
Fe_2O_3	-	-	86.58	63.08	-	-	-	-
MnO	0.54	0.70	0.34	0.22	0.23	0.00	0.16	0.02
P_2O_5	0.04	0.00	0.02	0.12	0.23	0.01	0.23	0.06
Total	100.00	100.00	100.00	100.00	100.00	100.00	100.00	100.00

Extended Data Figure 6 | Frictional melt chemistry. a, BSE image of the different phases and textures observed in the products of the rotary shear experiments, along with eight numbered locations of geochemical analyses acquired with the EPMA. **b**, Normalized geochemical composition of major elements for each analysis. Comparison of the chemical analyses with the textures reveals the variable heterogeneity of the rock products by frictional melting. Analyses 1 and 2 present pyroxene crystals in the seemingly undisturbed host rock and as fragments in the melt zone respectively; they do not show any degree of contamination. Similarly, analysis 3 presents a Fe-oxide crystal and analyses 6 and 8 present plagioclase crystals in the host rock which have not been chemically altered by the products of frictional melting. Analysis 4 presents a protomelt consisting of orthopyroxene with high concentration of Fe-oxide. Analysis 5 also presents a protomelt but this time the chemical composition, and in particular the intermediate concentrations of MgO, CaO and FeO, suggests that it is a mixing product of molten plagioclase and orthopyroxene crystals in a ratio nearing 1:1. Analysis 7 presents the geochemistry of the more homogenized central frictional melt zone, resulting from the mixing of the molten crystals described above.

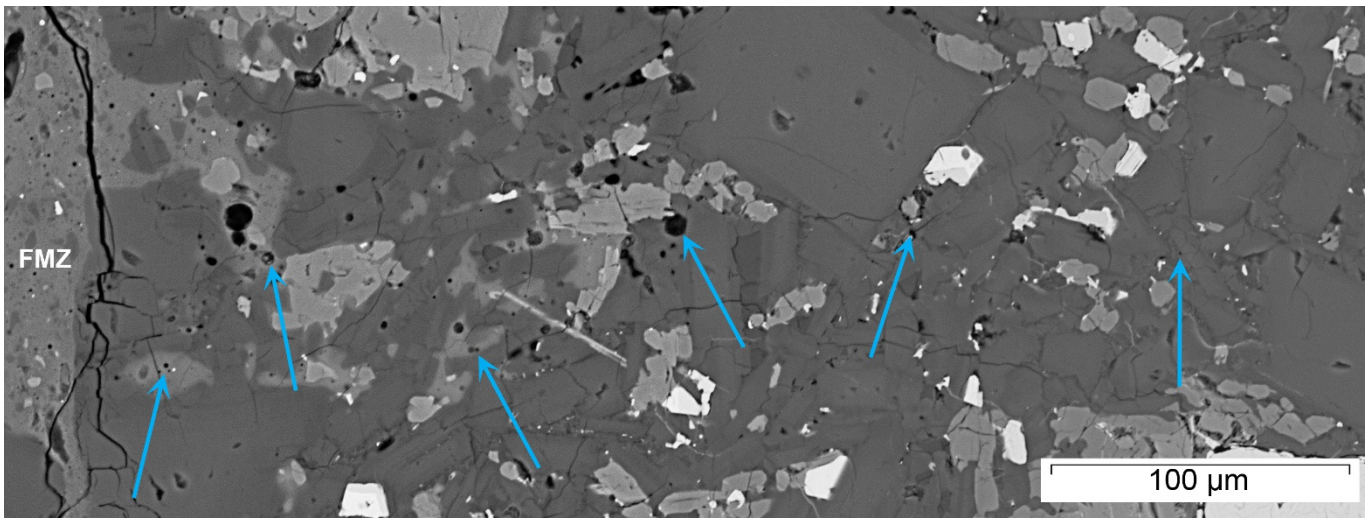

Extended Data Figure 7 | Vesicularity gradients developed in the interstitial glass along the edge of the FMZ. Blue arrows indicate vesicles. We observe no vesicles in the interstitial glass away (>0.4 mm) from the slip zone, and hence no vesicles in the pre-experimental sample.

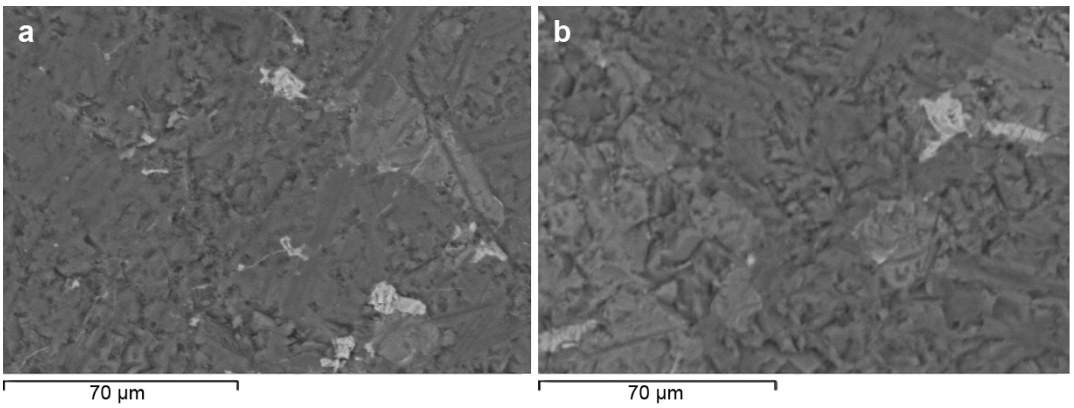

Extended Data Figure 8 | SEM images showing the texture of dome rocks unchanged by subjecting them to 850 °C. a, Heat applied for 30 min. **b**, Heat applied for 15 h. In either case, we note no new, spherical vesicles developed in the interstitial glass. This observation is consistent with the fact that the sample density did not change, as determined by helium pycnometry. This observation indicates that even at atmospheric pressure, water is unable to exsolve at magmatic temperature, suggesting that high heat input is necessary to lower the solubility and increase diffusivity to trigger vesiculation.